Characterization of Quality-Factor Tunable Integrated Silicon Microtoroidal Resonators

Jin Yao, David Leuenberger and Ming C. Wu
Berkeley Sensor & Actuator Center (BSAC) and Dept. Electrical Engineering and Computer Sciences, University of California Berkeley, Berkeley, California 94720, USA

ABSTRACT

Microresonators are basic building blocks for compact photonic integrated circuits (PICs). The performance of the microresonators depends on their intrinsic and loaded quality factors (Q). Here we demonstrate the optical characterization of a single crystalline silicon microtoroidal resonator with integrated MEMS-actuated tunable optical coupler. The device is realized on a two-layer silicon-on-insulator (SOI) structure. It is fabricated by combining hydrogen annealing and wafer bonding processes. The device has been demonstrated to be operated in all three coupling regimes: under-coupling, critical coupling, and over-coupling. At an actuation voltage of 114 V, the extinction ratio at the resonant wavelength of 1548.18 nm reaches 22.4 dB. To characterize these quality-factor tunable microtoroidal resonators, we have also developed a comprehensive model based on time-domain coupling theory. The intrinsic and loaded Qs are extracted by fitting the experimental curves with the model. The intrinsic Q is 110,000. And the loaded Q is continuously tunable from 110,000 to 5,400. This device has potential applications in variable bandwidth filters, reconfigurable add-drop multiplexers, and optical sensors.

Keywords: Optical resonators, integrated optics, tunable coupling, waveguide coupler, surface roughness

1. INTRODUCTION

Optical microresonators are key enabling building blocks for compact filters [1], add-drop multiplexers [2], optical dispersion compensators [3], delay lines [4], electro-optic modulators [5], lasers [6], nonlinear optical devices [7], and optical sensors [8, 9]. The performance of microresonators depends on their intrinsic and loaded quality factors (Q), which is achieved by controlling the coupling ratio between the coupler and the resonator. Microfabrciated resonators with very high Q has been demonstrated in SiO_2 [10] and Si [11]. To achieve optimum performance, the coupling ratio needs to be precisely controlled [12]. Previously this has been achieved by adjusting prism couplers in fused silica microsphere resonators [13] or using piezo-controlled micropositioners to move tapered fiber couplers [14-16]. However, such setups are bulky and cannot be integrated. In microresonators with integrated waveguides, the coupling ratio is determined by the fabrication process [17]. The loaded Q and its relation with the intrinsic Q cannot be controlled precisely. Some trimming processes have been proposed to control the resonance frequency but not the coupling [18, 19].

Recently, microresonators with tunable coupling ratios have been reported [20-23]. A Mach-Zehnder interferometer (MZI) has been integrated with a racetrack resonator [20]. The resonator can operate in all coupling regimes (uncoupled, under-, critical, or over-coupled). An intrinsic Q of 1.9×10^4 and an ON-OFF ratio of 18.5dB have been achieved. However, the circumference of the resonator is rather large (1430 μm) due to the long MZI structure, which limit the free spectral range and footprint it can achieve. Also, microfluidic approach has been employed to tune both the resonance wavelength and the coupling ratio of low-index SU8 microring resonators [23]. The refractive index of the liquid media was varied by mixing two different liquids. Critical coupling with an extinction ratio of 37 dB have been attained. However, index variation is small (~ 0.04), which limits the tuning range. In addition, and the tuning speed is slow (~ 2 sec) and the fluidic packaging is bulky in terms of integrated circuits. Previously, we have reported the first silicon microdisk resonator with integrated micro-electro-mechanical-systems (MEMS) tunable coupler [21, 22]. By physically changing the gap spacing between the waveguide and the resonator, coupling ratio can be varied from 0 to 34% and a high Q (100,000) have been achieved simultaneously. Tunable dispersion compensators (185 ps/nm to 1200

Integrated Optics: Devices, Materials, and Technologies XI, edited by Yakov Sidorin, Christoph A. Waechter,
Proc. of SPIE Vol. 6475, 647502, (2007) · 0277-786X/07/$18 · doi: 10.1117/12.699847

Downloaded from SPIE Digital Library on 23 Nov 2009 to 169.229.32.136. Terms of Use: http://spiedl.org/terms

ps/nm) have also been demonstrated [22]. However, in the microdisk resonators there is lack of radial mode control, which could produce additional resonances due to high order modes.

In this paper, we report on the optical characterization of a single crystalline silicon microtoroidal resonator with MEMS tunable optical coupler. Microtoroidal resonators offer tighter confinement of the optical mode and eliminate multiple radial modes observed in microdisks. Previously, microtoroidal resonators have been made in SiO_2 by thermal reflow [10], however, such process can not be applied to single crystalline structures. Instead, we use hydrogen annealing to create three-dimensional toroidal structures while preserving the single crystalline quality [24] and the smooth surface for the high optical performance. All three coupling regimes have been demonstrated, with the loaded Q tunable from 110,000 to 5,400.

2. DEVICE DESIGN AND FABRICATION

The schematic of the tunable integrated microtoroidal resonator is shown in Fig. 1(a). It is designed on a two-layer silicon-on-insulator (SOI) structure. Two suspended waveguide couplers are vertically aligned to a microtoroidal resonator. The microtoroid and the fixed electrodes of the MEMS actuators are integrated on the lower SOI layer, while the suspended waveguides are integrated on the upper SOI. The initial spacing between the microtoroid and the waveguides is 1 μm. This design ensures that there is negligible coupling at zero bias. By increasing voltage bias between the waveguide and the fixed electrodes, the suspended waveguide is pulled down towards the microtoroid, increasing the optical coupling, as illustrated in Fig. 1(a). This design enables the microtoroidal resonator to be biased in all coupling regimes: under-coupling, critical coupling, and over-coupling, and decoupled from the waveguide bus. The MEMS actuator design principles have been reported in [22].

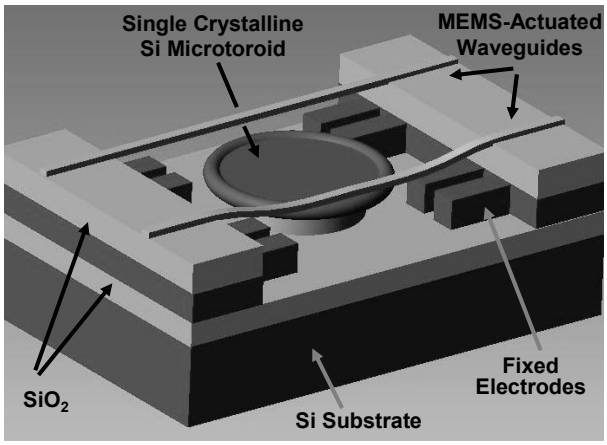

Figure 1(a). Schematic of the microtoroidal resonator with integrated MEMS tunable couplers. The lower waveguide is pulled downward by biased actuation to increase coupling, while the upper waveguide remains straight (uncoupled).

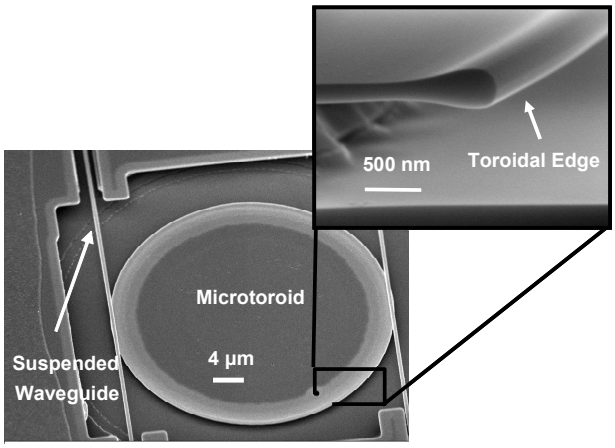

Figure 1(b). SEM of a fabricated microtoroidal resonator and the integrated waveguides. The inlet showing the cross-sectional view of the microtoroid.

The vertically coupled tunable microresonator is fabricated on a two-layer SOI using wafer bonding process. The detailed fabrication process is reported elsewhere [25]. The scanning electron micrograph (SEM) of the fabricated device is shown in Fig. 1(b). The dimensions of the waveguides are measured to be 0.69μm wide and 0.25μm thick, very close to the design parameters. In addition to creating toroidal shape, the hydrogen annealing also reduces the surface roughness (to < 0.26 nm as reported in [26]), which is critical to attain high Q. The resonator exhibits a smooth sidewall.

3. OPTICAL CHARACTERIZATION

The optical characterization of the tunable microtoroidal resonator is performed by using a measurement setup with both a broadband amplified spontaneous emission (ASE) source (OpticWave Communications Mini BLS-C-13) shown as method (A) in Fig. 2, and a tunable laser (Agilent 8164A) shown as method (B) in Fig. 2.

Downloaded from SPIE Digital Library on 23 Nov 2009 to 169.229.32.136. Terms of Use: http://spiedl.org/terms

Through the polarization maintaining lensed fibers the incident light is edge coupled to the integrated waveguides, as the setup shows in Fig. 2. A calibrated optical power meter (HP 8153A) and an optical spectrum analyzer (OSA) (ANDO AQ6317B) are used at the output to measure the transmitted power. In method (A), the ASE provides a broadband source for fast and overall spectral measurement. We have used TE-polarized input, which is attained by a linear polarizer and a polarization controller.

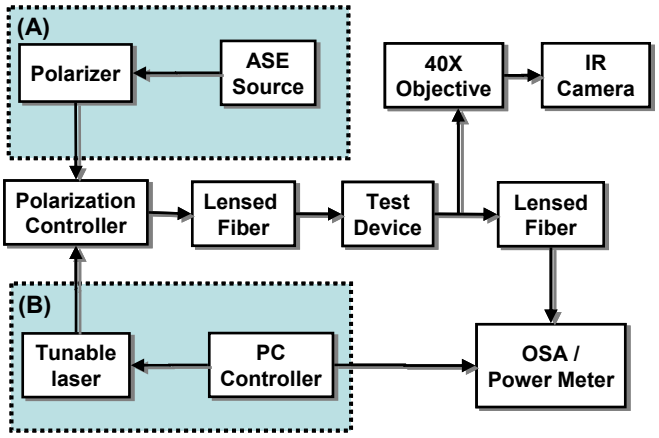

Figure 2. Experimental setup for optical characterization with method (A) ASE broadband measurement and method (B) laser sweeping

While the waveguide is grounded, a voltage bias is applied to the fixed electrodes to actuate the waveguide. At zero bias, almost 100% of the light is transmitted to the output port. With increasing bias, sharp dips gradually appear in the transmission spectrum, as shown in Fig. 3. Each dip corresponds to a resonant wavelength. The free spectral range (FSR) of the TE mode is measured to be 5.2 nm. The small ripples are due to the reflections from the cleaved facets (Fabry-Perot effect). By anti-reflection coating the facets, these ripples can be eliminated to utilize the tunable microresonators in tunable applications such as bandwidth-tunable filters [27]. Only one resonance peak is observed within each FSR, confirming the successful suppression of multiple radial modes observed in microdisk resonators.

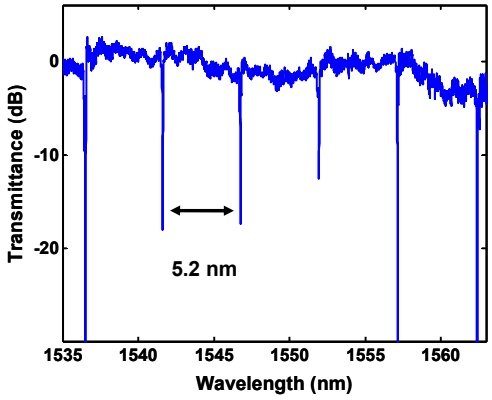

Figure 3. Measured optical spectrum of a microtoroidal resonator at a bias voltage of 64V. The measured free spectral range (FSR) of the TE mode is 5.2 nm.

With the integrated tunable waveguide coupler, the microtoroidal resonator was able to be continuously operated in all coupling regimes. At low voltage, the microresonator is in under-coupled regime. Fig. 4(a) shows the normalized transmission spectra of the resonator around one of the resonant wavelengths at 1548.2 nm at bias voltages of 51.0, 56.0, and 64.8V, respectively. As the voltage increases, the dip becomes larger at resonance, due to the fact that the optical coupling becomes stronger. In the under-coupling regime (V_{bias} < 114V), the transmittance decreases continuously with increasing voltage. The transmittance reaches a minimum at critical coupling (V_{bias} = 114V). The extinction ratio is

Downloaded from SPIE Digital Library on 23 Nov 2009 to 169.229.32.136. Terms of Use: http://spiedl.org/terms

measured to be 22.4 dB at critical coupling. The resonator is operated in the over-coupling regime when the voltage is further increased. Fig. 4(b) shows the normalized transmittance at the resonant wavelength changes as a function of the applied voltage, indicating the three coupling regimes.

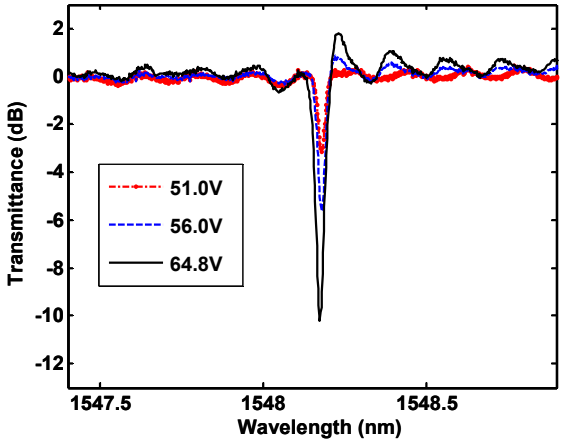

Figure 4(a). Measured normalized optical spectra of a microtoroidal resonator at bias voltages of 51.0, 56.0, and 64.8V.

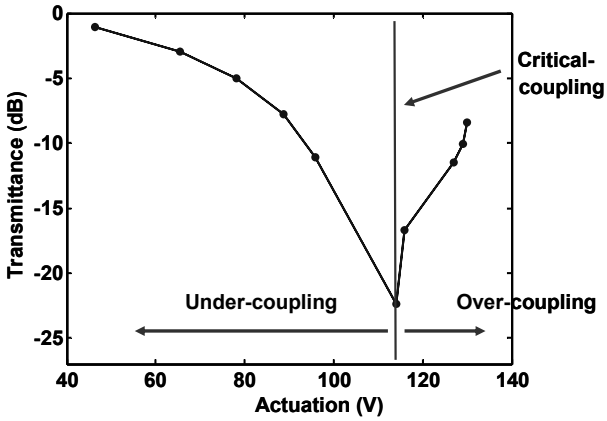

Figure 4(b). Normalized transmittance at resonance versus actuation voltage. The microresonator can be tuned continuously from under-coupling regime to over-coupling regime.

4. THEORETICAL MODELING

To further analyze the characterization measurement, a theoretical model is built. According to the time-domain coupling theory [1], the optical transfer function of the microresonator can be expressed as a function of resonant frequency (ω_0) and amplitude decay time constants, τ_0 and τ_e, due to intrinsic loss and external coupling, respectively:

$$t_{res} = \frac{j(\omega-\omega_0)+\frac{1}{\tau_0}-\frac{1}{\tau_e}}{j(\omega-\omega_0)+\frac{1}{\tau_0}+\frac{1}{\tau_e}} \tag{1}$$

where t_{res} is the amplitude transfer function of the microresonator.

Alternatively, the transfer function can also be expressed in terms of the intrinsic quality factor, Q_0, and the external quality factor, Q_e:

$$t_{res} = \frac{2j\left(\frac{\lambda_0-\lambda}{\lambda}\right)+\left(\frac{2}{Q_0}-\frac{1}{Q_L}\right)}{2j\left(\frac{\lambda_0-\lambda}{\lambda}\right)+\left(\frac{1}{Q_L}\right)} \tag{2}$$

where $Q_0=\omega_0\tau_0/2$, $Q_e=\omega_0\tau_e/2$, and the loaded quality factor Q_L is defined as

$$\frac{1}{Q_L}=\frac{1}{Q_0}+\frac{1}{Q_e}, \tag{3}$$

We have developed a comprehensive model that includes both the effect of the microresonator and the FP ripples, so that to more precisely model the measured spectrum and more accurately extract the Q values of the resonator, particularly when the resonance peak is small. The measured spectra here are complicated by the Fabry-Perot resonance between the two cleaved facets, as illustrated in Fig. 5.

Downloaded from SPIE Digital Library on 23 Nov 2009 to 169.229.32.136. Terms of Use: http://spiedl.org/terms

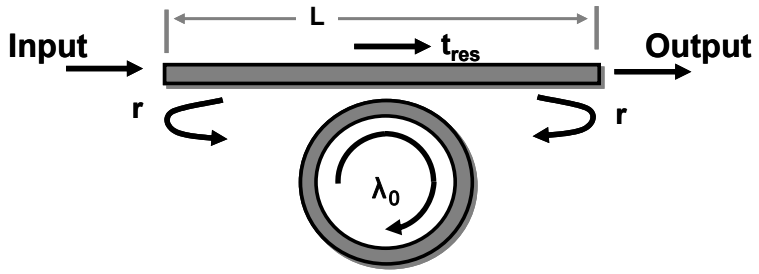

Figure 5. Schematics illustrating the interaction between the microresonator and the Fabry-Perot resonance of the coupling waveguide.

Hence the total transmission t_{tot} is derived as a summation of multiple transmissions through the waveguide, as shown in equation (4):

$$\begin{aligned} t_{tot} &= (1-r)^2 \cdot \exp(-\alpha L) \cdot \exp\left(jkLn_{eff}\right) \cdot t_{res} \\ &+ (1-r)^2 \cdot r^2 \cdot \exp(-3\alpha L) \cdot \exp\left(j(3kLn_{eff} + 2\phi_R)\right) \cdot t_{res}^3 \\ &+ (1-r)^2 \cdot r^4 \cdot \exp(-5\alpha L) \cdot \exp\left(j(5kLn_{eff} + 4\phi_R)\right) \cdot t_{res}^5 \\ &+ \cdots \end{aligned} \tag{4}$$

where r is the amplitude reflection coefficient at the facet of the silicon waveguide, α is the optical loss per unit length in the waveguide, L is the length of the waveguide, k is the free-space propagation constant, n_{eff} is the effective refractive index of the Si waveguide, and ϕ_R is the optical phase change at the reflection per interface. Since there is a π phase shift at the reflection interface, the total transmission t_{tot} can be simplified as the following:

$$\begin{aligned} t_{tot} &= (1-r)^2 \cdot \exp(-\alpha L) \cdot \exp\left(jkLn_{eff}\right) \cdot t_{res} \cdot \\ &\{1 + r^2 \cdot \exp(-2\alpha L) \cdot \exp\left(j2kLn_{eff}\right) \cdot t_{res}^2 \\ &+ r^4 \cdot \exp(-4\alpha L) \cdot \exp\left(j4kLn_{eff}\right) \cdot t_{res}^4 + \cdots\} \\ &= a_0 \left(1 + q + q^2 + q^3 + \cdots\right) \\ &= \frac{a_0}{1-q} \end{aligned} \tag{5}$$

where $a_0 = (1-r)^2 \cdot \exp(-\alpha L) \cdot \exp\left(jkLn_{eff}\right) \cdot t_{res}$, and $q = r^2 \cdot \exp(-2\alpha L) \cdot \exp\left(j2kLn_{eff}\right) \cdot t_{res}^2$.

In this derivation, we have assumed the backscattering effect is small and can be neglected. The total intensity transmittance is then given by

$$T_{res} = \left|t_{tot}\right|^2 \tag{6}$$

To include the effect of waveguide dispersion, the phase factor kLn_{eff} is replaced by

$$\begin{aligned} \phi &= kL\left[n_{eff} + \frac{dn}{d\lambda}(\lambda - \lambda_0)\right] \\ &= kLn_{eff}\left[1 + \frac{dn}{d\lambda}\frac{1}{n_{eff}}(\lambda - \lambda_0)\right] \\ &= kLn_{eff}\left[1 + D_\lambda(\lambda - \lambda_0)\right] \end{aligned} \tag{7}$$

Downloaded from SPIE Digital Library on 23 Nov 2009 to 169.229.32.136. Terms of Use: http://spiedl.org/terms

where $D_\lambda = \frac{dn}{d\lambda}\frac{1}{n_{eff}}$.

With this model, the quality factors, Q_0 and Q_L, are extracted from the measured optical spectra by least-square-fitting to the model. Fig. 6 shows the measured and the fitted spectra around the resonance peak at 1548.2 nm when the resonator is operated in (a) decoupled, (b) under-coupled, and (c) over-coupled regimes, respectively. The experimental data agree very well with the theoretical model.

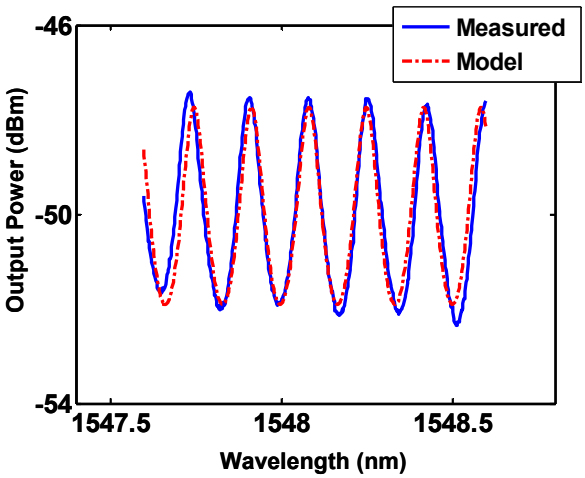

Figure 6(a) Measured and modeled spectra at 0V (microresonator is decoupled).

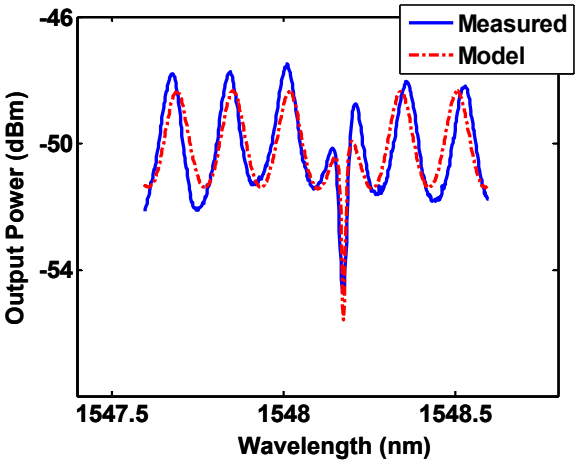

Figure 6(b). Measured and modeled spectra at 64.8V (microresonator is under-coupled)

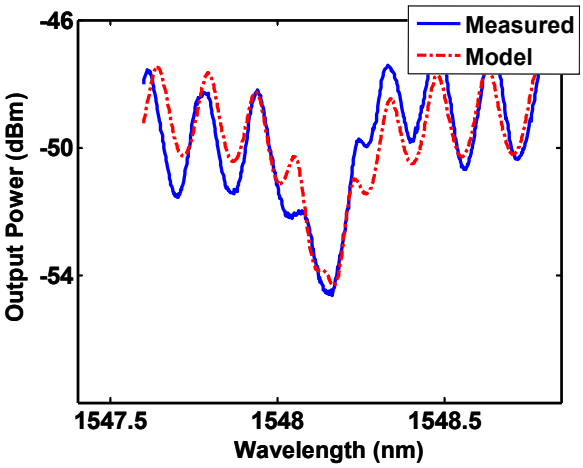

Figure 6(c). Measured and modeled spectra at 130V (microresonator is over-coupled)

From the fitted spectral response, the intrinsic quality factor, Q_0, of the microtoroidal resonator is extracted to be 110,000. The loaded Q, Q_L, is continuously tunable from 110,000 to 5,400, exhibiting a tuning ratio of more than 20:1. Compare to the model used for lumped resonator alone in [28], the model described in this paper not only fit the resonance peak but also the ripples due to the Fabry-Perot resonance. It has further explained and matched the ripples around the resonant wavelengths where the lumped model with normalized spectrum could not.

Downloaded from SPIE Digital Library on 23 Nov 2009 to 169.229.32.136. Terms of Use: http://spiedl.org/terms

With the optical characterization, these tunable microresonators described in this paper can be cascaded to form reconfigurable optical add-drop multiplexers, wavelength-selective switches and crossconnects. It can also be used for bandwidth-tunable filters in dynamic optical networks. With the successful suppression of multiple radial modes, we have demonstrated the microtoroidal resonator to have even larger bandwidth tuning range [27] than the microdisk-based filters in [29].

5. CONCLUSION

We have successfully performed the optical characterization of a novel single crystalline silicon microtoroidal resonator with MEMS-actuated tunable optical coupler. It is fabricated by combining the hydrogen annealing and the wafer bonding processes. We have achieved an intrinsic quality factor (Q) of 110,000 for a fabricated 39-μm-diameter resonator with a toroidal radius of 200 nm. The device is able to operate in all three coupling regimes: under-coupling, critical coupling, and over-coupling. We have attained 22.4 dB extinction ratio at the resonant wavelength of 1548.18 nm with an actuation voltage of 114 V. The resonator can also be decoupled from the waveguide, to allow them to be cascaded without loading the waveguides. We have also developed a detailed model combining the resonator by time-domain coupling theory with the Fabry-Perot resonance of the waveguide. The experimental and theoretical results agree very well. The intrinsic Q is extracted to be 110,000. The loaded Q is continuously tunable from 110,000 to 5,400. This device has potential applications in variable bandwidth filters, reconfigurable add-drop multiplexers, wavelength-selective switches and crossconnects, and optical sensors.

ACKNOWLEDGMENT

The authors would like to thank the staff of the Microfabrication Lab at the University of California, Berkeley. Part of the fabrication process was completed at Stanford Nanofabrication Facility, Stanford University. We like to acknowledge the assistance from Maurice Stevens and Mahnaz Mansourpour, We also like to thank Dr. Sagi Mathai and Dr. Xiaofan Meng from the University of California, Berkeley for helpful discussions and technical assistance.

REFERENCES

1. B. E. Little, S. T. Chu, H. A. Haus, J. Foresi, and J.P. Laine, “Microring resonator channel dropping filters,” *Journal of Lightwave Technology*, 15(6), 998-1005 (1997).
2. B. E. Little, S. T. Chu, W. Pan, and Y. Kokubun, "Microring resonator arrays for VLSI photonics," *IEEE Photonics Technology Letters*, 12, 323-325, (2000).
3. C. K. Madsen, G. Lenz, A. J. Bruce, M. A. Cappuzzo, L. T. Gomez, T. N. Nielsen, L. E. Adams, and I. Brenner, "An all-pass filter dispersion compensator using planar waveguide ring resonators," in *OFC/IOOC'99 Optical Fiber Communication Conference and the International Conference on Integrated Optics and Optical Fiber Communications* (Cat. No.99CH36322) 99-101 (1999).
4. G. Lenz, B. J. Eggleton, C. K. Madsen, and R. E. Slusher, “Optical delay lines based on optical filters,” *IEEE Journal of Quantum Electronics*, 37, 525-532 (2001).
5. Q. Xu, B. Schmidt, S. Pradhan, and M. Lipson, “Micrometre-scale silicon electro-optic modulator,” *Nature*, 435, 325-327 (2005).
6. C. Seung June, K. Djordjev, C. Sang Jun, and P. D. Dapkus, "Microdisk lasers vertically coupled to output waveguides," *IEEE Photonics Technology Letters*, 15, 1330-1332 (2003).
7. T. J. Kippenberg, S. M. Spillane, D. K. Armani, and K. J. Vahala, “Ultralow-threshold microcavity Raman laser on a microelectronic chip,” *Optics Letters*, 29, 1224-1227 (2004).
8. F. Vollmer, S. Arnold, D. Braun, I. Teraoka, and A. Libchaber., “Multiplexed DNA Quantification by Spectroscopic Shift of Two Microsphere Cavities,” *Biophysical Journal*, 85, 1974-1979 (2003).
9. A. M. Armani, and K. J. Vahala, “Heavy water detection using ultra-high-Q microcavities,” *Optics Letters,* 31(12), 1896-1898 (2006).
10. D. K. Armani, T. J. Kippenberg, S. M. Spillane, and K. J. Vahala, “Ultra-high-Q toroid microcavity on a chip”, *Nature*, 421, 925-929 (2003).

Downloaded from SPIE Digital Library on 23 Nov 2009 to 169.229.32.136. Terms of Use: http://spiedl.org/terms

11. M. Borselli, T. Johnson, O. Painter, “Beyond the Rayleigh scattering limit in high-Q silicon microdisks: theory and experiment,” *Optics Express*, 13(5), 1515-1530 (2005).
12. A. Yariv, “Critical Coupling and Its Control in Optical Waveguide-Ring Resonator Systems, *IEEE Photonics Technology Letters,* 14, 483-485 (2002).
13. V. B. Braginsky, M. L. Gorodetsky, and V. S. Ilchenko, “Quality-factor and nonlinear properties of optical whispering-gallery modes,” *Phys. Lett. A* 137, 393-397 (1989).
14. J. C. Knight, G. Cheung, F. Jacques, and T. A. Birks, "Phase-matched excitation of whispering-gallery-mode resonances by a fiber taper," *Opt. Lett.* 22, 1129-1131 (1997).
15. M. Cai, O. Painter, and K. J. Vahala, “Observation of Critical Coupling in a Fiber Taper to a Silica-Microsphere Whispering-Gallery Mode System,” *Phys. Rev. Lett.* 85, 74-77 (2000).
16. M. Borselli, K. Srinivasan, P. E. Barclay, and O. Painter, “Rayleigh scattering, mode coupling, and optical loss in silicon microdisks,” *Appl. Phys. Lett.* 85, 3693–3695 (2004).
17. L. Martinez, and M. Lipson, “High confinement suspended micro-ring resonators in silicon-on-insulator,” *Optics Express*, 14(13), 6259-6263 (2006).
18. S. T. Chu, W. Pan, S. Sato, T. Kaneko, Y. Kokubun, and B. E. Little, “Wavelength trimming of a microring resonator filters by means of a UV sensitive polymer overlay,” *IEEE Photonics Technology Letters*, 11(6), 688-690 (1999).
19. D. K. Sparacin, J. P. Lock, C. Hong, K. K. Gleason, L. C. Kimerling, J. Michel, “Trimming of Microring Resonators Using Photo-Oxidation of a Plasma-Polymerized Organosilane Cladding Material,” *Optics Letters*, 30(17), 2251-2253 (2005).
20. W. M. J. Green, R. K. Lee, G. DeRose, A. Scherer, and A. Yariv, "Hybrid InGaAsP-InP Mach-Zehnder Racetrack Resonator for Thermooptic Switching and Coupling Control," *Opt. Express* 13, 1651-1659 (2005).
21. M-C. M. Lee and M. C. Wu, “MEMS-Actuated Microdisk Resonators with Variable Power Coupling Ratios,” *IEEE Photonics Technology Letters,* 17, 1034-1036 (2005).
22. M-C. M. Lee and M. C. Wu, “Tunable coupling regimes of silicon microdisk resonators using MEMS actuators”, *Optics Express*, 14(11), 4703-4712 (2006).
23. U. Levy et al., “On-chip microfluidic tuning of an optical microring resonator,” *Appl. Phys. Lett.* (88), 111107-111109 (2006).
24. M-C. M. Lee and M. C. Wu, "Thermal Annealing in Hydrogen for 3-D Profile Transformation on Silicon-on-Insulator and Sidewall Roughness Reduction," *Journal of Microelectromechanical Systems*, 15(2), 338-343 (2006).
25. J. Yao, M-C. M. Lee and M. C. Wu, “Hydrogen Annealing and Bonding Processes for Integrated MEMS Tunable Microtoroidal Resonators,” to be submitted to *Journal of Microelectromechanical Systems.*
26. M-C. M. Lee, J. Yao and M. C. Wu, “Silicon Profile Transformation and Sidewall Roughness Reduction Using Hydrogen Annealing,” in *18th IEEE International Conference on Micro Electro Mechanical Systems*, Miami, USA, 596-599 (2005).
27. J.Yao and M. C. Wu, “Bandwidth-Tunable Add-Drop Filters Based on MEMS-Actuated Single-Crystalline Silicon Microtoroidal Resonators,” submitted to CLEO 2007.
28. J. Yao, M-C. M. Lee, D. Leuenberger and M. C. Wu, “Silicon Microtoroidal Resonators with Integrated MEMS Tunable Optical Coupler”, presented at *IEEE Optical Micro-Electro-Mechanical-System,* MA7, Big Sky MT, USA, 2006.
29. J. Yao, M-C. M. Lee, D. Leuenberger and M. C. Wu, “Wavelength- and Bandwidth-Tunable Filters Based on MEMS-actuated Microdisk Resonators,” in *Optical Fiber Communication Conference, 2006 and the 2006 National Fiber Optic Engineers Conference,* Anaheim, USA, 2006.

Downloaded from SPIE Digital Library on 23 Nov 2009 to 169.229.32.136. Terms of Use: http://spiedl.org/terms